CLM-R 267

CLM-R 267

UKAEA

Report

A RATE LIMITED MFCI MODEL FOR SODIUM

D. F. FLETCHER

CULHAM LABORATORY
Abingdon, Oxfordshire
1986

C.18

Available from H. M. Stationery Office

Price £4.00

CLM-R267

CURLIM

A RATE LIMITED MFCI MODEL FOR SODIUM

Part II: Model Improvements and Hicks-Menzies Calculations

D.F.Fletcher
UKAEA, Culham Laboratory,
Abingdon, Oxon, OX14 3DB, U.K.

Abstract

In this paper we describe modifications to CURLIM, a rate limited MFCI model for sodium. The modifications include improvements to the heat transfer model and the incorporation of a model of heat loss from the interaction zone. In addition, we modify the treatment of returning rarefaction waves during the acoustic loading stage. Finally, CURLIM is used to perform Hicks-Menzies calculations using the latest equation of state for sodium.

May, 1986.

ISBN 085311 1510

Contents

Nomenclature

A	Surface area
a	$\equiv 1 - \delta/R$
c	sound speed or specific heat capacity
D_H	hydraulic diameter of sodium slug
E_∞	Total excess heat content of melt (above sodium saturation temperature)
h	heat transfer coefficient
k	thermal conductivity
L	slug length
m	mass
P	pressure
Q	heat flux per unit area
q	heat flux or heat flux per unit mass of sodium
R	particle radius
r	radial coordinate
S	interfacial area between slug and MFCI zone
T	temperature
t	time
v	velocity
x	quality or mass fraction
z	acoustic impedance

Greek symbols

α	thermal diffusivity
β_s	isentropic compressibility
δ	thermal boundary-layer thickness
ρ	density
ν	specific volume
τ_{ac}	acoustic relief time ($\equiv 2L/c$)
τ_f	fragmentation time constant
τ_h	heat transfer time constant
η	efficiency
γ	vapour film thickness
ε	emissivity
σ	Stefan-Boltzmann constant

Subscripts

cen	property at sphere centre
cut	value at heat transfer cut-off
init	value after constant volume mixing
m	melt
mix	mixture property
mod	modified Hicks-Menzies value
s	sodium
side	sidewalls
slug	slug property
top	interface between slug and MFCI zone
v	vapour
0	initial value

overbar denotes spatial average

dot denotes time derivative

1. Introduction

In a previous paper [1] a rate limited model for molten fuel-coolant interactions in sodium, named CURLIM, was described. The model assumes a one-dimensional geometry with an interaction zone surmounted by a sodium slug. Expansion of the heated sodium in the interaction zone sets the slug in motion, which in turn compresses isentropically a fixed mass of overgas. The model was used to examine the effect of varying uncertain parameters and it was concluded that the simulation of heat transfer is the most sensitive part of the model.

In this paper we describe some modifications and improvements to the basic model. In section 2 an improved treatment of the modelling of rarefaction waves during the acoustic stage of the slug dynamics is described. In section 3 a diffusivity limited heat transfer model is implemented and investigated, and a model which allows for a finite fragmentation rate is proposed. A mechanistic model of heat transfer during the two phase stage is developed and investigated. The modelling of heat loss from the interaction zone to its surroundings is examined in section 4. In section 5 an option which allows the model to be used for carrying out improved Hicks-Menzies thermodynamic limit calculations is described. Finally, we draw some conclusions in section 6.

2. An Improved Acoustic Loading Model

In the earlier report describing CURLIM [1] the hydrodynamic modelling of the sodium slug was discussed in detail. In this section we present an improved treatment of the modelling of the slug behaviour at the time of the return of the rarefaction wave to the interaction zone. For $t < \tau_{ac}$ (i.e. for times before a rarefaction wave returns) the model is unchanged. It is easily shown (see Appendix 1) that the approach used in CURLIM and by other workers (e.g. [2]) models the rarefaction wave as being reflected at the MFCI/slug interface and not transmitted as claimed.

The behaviour of an acoustic wave at an interface depends on the relative acoustic impedances of the two media. The acoustic impedance is defined by

$$z = \rho c \tag{2.1}$$

The sound speed is calculated from the isentropic compressibility using

$$c = \frac{1}{\sqrt{\rho \beta_s}} \tag{2.2}$$

and is found to depend strongly on temperature but not pressure for most materials [3]. Thus for the purpose of the present calculations we assume that the sound speed is a function of temperature only and use saturation line values for sodium. Table 2.1 below shows the acoustic impedance of sodium and uranium dioxide as a function of temperature. The necessary data was taken from references 4 and 5.

Material	Temperature (K)	Acoustic Impedance kg/m^2s
UO_2	3500	1.57×10^7
UO_2	3120	1.80×10^7
sodium	2000	7.55×10^5
sodium	1156	1.55×10^6

TABLE 2.1: The Acoustic Impedance of Uranium Dioxide and Sodium as a function of Temperature

We now determine the acoustic impedance of a mixture of the two components. Let x be the mass fraction of component 1, then

$$\nu_{mix} = x\nu_1 + (1-x)\nu_2 \tag{2.3}$$

where x is <u>fixed</u>. It is straightforward to show that

$$z_{mix} = (x/z_1^2 + (1-x)/z_2^2)^{-1/2} \tag{2.4}$$

Table 2.2 below gives the acoustic impedances for various mixtures of liquid sodium at 2000K with UO_2 at 3500K, and the ratio of these to the acoustic impedance of a sodium slug at 1156K.

Mass fraction of UO_2	z_{mix} (kg/m^2s)	z_{mix}/z_{slug}
0	0.76×10^6	0.48
0.25	0.87×10^6	0.56
0.5	1.07×10^6	0.69
0.75	1.50×10^6	0.97
1.0	15.7×10^6	10.1

TABLE 2.2: The Acoustic Impedance of mixtures of Sodium and Uranium Dioxide of various proportions.

Discussions of the relationship between the ratio of the acoustic impedances and the behaviour of sound waves are given in references 6 and 7. For $z_{mix}/z_{slug} = 1$ the rarefaction wave will be transmitted perfectly. For $z_{mix}/z_{slug} \ll 1$ there is perfect reflection with a rarefaction wave being reflected as a shock wave and for $z_{mix}/z_{slug} \gg 1$ the rarefaction wave is reflected as a rarefaction wave. Thus we see from the above data that the assumption of perfect transmission is the best simple choice unless the mixture consists almost entirely of melt. Only in the case when vapour is present will z_{mix}/z_{slug} be low enough to cause almost total reflection of the rarefaction wave.

At the boundary between the slug and the MFCI zone the particle velocity is given by [6,7]

$$v = \frac{P(t) - P_o}{z_{slug}} \qquad (2.5)$$

before the return of the rarefaction wave. Upon return of the rarefaction wave an additional velocity $\frac{P(t-\tau) - P_o}{z_{slug}}$ is added to this, [6,7] giving

$$v = \frac{1}{z_{slug}} \left(P(t) + P(t-\tau) - 2P_o\right) \qquad (2.6)$$

This increased particle velocity will lead to rapid depressurization of the interaction zone as expansion occurs. In reality the rarefaction wave would travel into the MFCI region forming an expansion fan which would be reflected at the base of the interaction zone, leading to a complex pressure distribution. In addition, non-homogeneity in the mixture would cause multiple reflections of the pressure waves. In the present model there is a uniform pressure in the interaction zone, so these detailed effects cannot be modelled. After each time-step a new spatially constant pressure is calculated and used to determine the interface velocity at the next timestep.

2.1 Application to CURLIM

The modification described in this section is only used when vapour has not formed before $t = \tau_{ac}$. For most of the calculations given in the earlier report [1] this modification has no effect, since vapour forms before $t = \tau_{ac}$. Only in cases where the heat transfer rate is low or the slug length is short (so that τ_{ac} is small) is the new treatment needed.

However, in these cases the modification was found to have a small effect. For example, for run 5 (using a heat transfer coefficient of 10^6 W/m^{2}K) the efficiency was changed from 8.17% to 8.38% and for run 16 (using a slug length of 0.2m) the efficiency was changed from 8.32% to 8.76%. Thus it may be concluded that the model assumptions are not sensitive to the choice of boundary conditions upon return of the rarefaction wave. The two versions differ only by the factor two multiplying the term in $P(t-\tau)$ for the reflection condition, compared to unity for the transmission condition. Thus, in the case of the reflection condition, the interface velocity is higher and vapour forms earlier leading to slightly lower efficiencies.

3. Improvements to the Modelling of Heat Transfer

In this section we modify the modelling of heat transfer in CURLIM. In Section 3.1 we describe a diffusivity limited heat transfer model which is used when the melt is in contact with high-density sodium. The model is formulated for the case of instantaneous fragmentation and results

obtained using CURLIM are described in Section 3.2. In Sections 3.3 and 3.4 we discuss the modelling of a finite fragmentation rate and suggest a form for a combined fragmentation/heat transfer model. In Section 3.5 we describe a mechanistic model for use in the two phase region.

3.1. A Diffusivity Limited Model of Heat Transfer

In the first version of CURLIM, heat transfer during the initial phase (when melt is in contact with high-density sodium) was modelled by assuming an arbitrary heat transfer coefficient. In this section we describe the implementation of a diffusivity limited heat transfer model. In this model heat transfer from the melt to the sodium is limited only by the thermal diffusivity of the melt.

The model is taken directly from a paper by Cho, Ivins and Wright [8]. It is applicable when all the melt is in the form of spheres with the same diameter, which were fragmented at the same time. The model is constructed from a solution of the conduction equation via the use of an integral method. Integrating the conduction equation with respect to r from 0 to R and assuming a constant thermal diffusivity gives

$$\frac{d}{dt}\int_0^R r^2\, T_m\, dr = \alpha_m\, R^2 \left[\frac{dT_m}{dr}\right]_{r=R} \qquad (3.1)$$

Equation (3.1) can then be solved to obtain the surface heat flux if a suitable temperature profile in the melt is assumed. The chosen profile is

$$\frac{T - T_s}{T_{m0} - T_s} = \begin{cases} \frac{R}{\delta}(1-r/R) & R-\delta \leqslant r < R \\ 1 & 0 \leqslant r \leqslant R-\delta \end{cases} \qquad (3.2)$$

which gives a linear profile over a boundary-layer of thickness δ. When the boundary-layer thickness becomes equal to the particle radius the temperature profile is taken to be linear over the entire sphere, so that

$$\frac{T - T_s}{T_{cen} - T_s} = 1 - r/R \qquad 0 \leqslant r \leqslant R \qquad (3.3)$$

These profiles are shown in figure 3.1. It should be noted that the sodium temperature is allowed to vary with time, so that the heat transfer rate is reduced as the sodium temperature increases. Substituting the chosen profiles into equation (3.1) gives the following equations

$$\frac{dT_s}{dt}\left[1-\tfrac{1}{4}(1+a+a^2+a^3)\right] + \frac{(T_{mo}-T_s)}{4}(1+2a+3a^2)\frac{da}{dt} = \frac{3\alpha_m}{R^2}\frac{(T_{mo}-T_s)}{a-1} \qquad (3.4)$$

and

$$\bar{T}_m = \frac{T_{mo}}{4}\left[1+a+a^2+a^3\right] + \frac{T_s}{4}\left[3-a-a^2-a^3\right] \qquad (3.5)$$

where $a = (1-\delta/R)$, for the boundary-layer stage, and

$$\frac{d\bar{T}_m}{dt} = \frac{12\alpha_m}{R^2}(T_s - T_{cen}) \qquad (3.6)$$

where

$$\bar{T}_m = 3/4\ T_s + 1/4\ T_{cen} \qquad (3.7)$$

for the developed stage.

The heat supplied to a unit mass of sodium is given by

$$q = -A\,k_m\frac{(T_{mo}-T_s)}{\delta\, m_s} \qquad (3.8)$$

during the boundary-layer phase and

$$q = -A\,k_m\frac{(T_{cen}-T_s)}{R\, m_s} \qquad (3.9)$$

during the developed phase.

3.2 Application to CURLIM

The single phase heat transfer model in CURLIM was replaced by the above model in a version of the code named CURLIM2. The incorporation of the extra differential equations into the model was straightforward. An arbitrarily small value for the boundary-layer thickness, δ, was chosen to start the calculation, since the model is only appropriate once a temperature gradient has developed. An initial value of $\delta = 0.01R$ was used and it was found that setting $\delta = 0.005R$ initially made only a small change to the solution. Calculations were made for the base case conditions (described in Appendix 1 of [1]) assuming instantaneous fragmentation to particle sizes of 250 μm and 100 μm. A summary of the results obtained is given in table 3.1 below, where they are compared with results obtained from the original model (using a single phase heat transfer coefficient of 10^7 W/m^{2}K).

Particle size (μm)	Model	Efficiency (%)	Peak Pressure (MPa)	$\bar{T}_m$ at the time of vapour formation (K)
250	OLD	8.37	449	2456
250	NEW	5.66	94.5	2760
100	OLD	8.46	639	2447
100	NEW	8.42	225	2492

Table 3.1: Comparison of results from the old and new heat transfer models.

The data in the above table show that for a particle size of 250 μm the efficiency is reduced from 8.37% to 5.66%. For a particle size of 100 μm the efficiency is virtually unchanged. The peak pressure is reduced in the calculations using the new model in both cases, showing that it gives a slower rate of heat release. However, because higher pressures cause more rapid expansion of the interaction zone this does not

necessarily result in lower efficiencies, since rapid heat transfer occurs for longer with the new model.

Figures 3.2 and 3.3 show temperature-pressure plots for the case of 250 μm particles for the old and new models, respectively. The figures show that not only are the peak pressures and efficiencies changed but also that the thermodynamic trajectories are very different. For the case of the new model the temperature of the sodium does not rise to as high values as for the old model. This is because heat transfer is reduced by the temperature gradient in the melt, as well as the increase in the temperature of the surroundings. This causes vapour to form earlier and at lower pressure so that the thermodynamic trajectory intersects the saturation line at a much lower temperature and specific volume.

This has implications on the influence of the possible metal-insulator transition in sodium. If the transition is assumed to occur at a specific volume of 2×10^{-3} m^3/kg, as in the earlier paper, it would have no effect on the calculation shown in figure 3.3, whereas it would affect the results of the simulation shown in figure 3.2. This highlights the importance of making a realistic simulation of the thermodynamic trajectory if the metal-insulator transition is to be modelled correctly.

3.3 The Framework Needed to Model Fragmentation

The model described above gives an upper bound for the rate of heat transfer but it has several limitations:

(i) it assumes instantaneous fragmentation of the melt;

(ii) no allowance is made for resistance to heat transfer between the melt and sodium.

To model a finite fragmentation rate it is necessary to allow for the different thermal boundary-layer thicknesses in the melt which has been fragmented at different times. Mathematically this implies that

$$q(t) = \int_0^t \dot{A}(t-\tau)\, Q\,(\tau)\, d\tau \qquad (3.10)$$

where: $\dot{A}(t)dt$ is the surface area of melt formed in time t to t + dt ;

$Q(t)$ is the heat flux per unit area from a particle which has been fragmented for a time t;
and, $q(t)$ is the heat flux to the sodium at time t.

Unfortunately, fragmentation and heat transfer both occur on millisecond timescales so it is not possible to simplify the convolution integral given above. Also it is not possible to determine a simple analytic expression for $Q(t)$ which allows for the reduction in heat transfer as temperature gradients develop in the melt and sodium. Thus it does not seem possible to improve the modelling of the heat transfer process within the framework of a simple parametric model without a considerable degree of simplification. A model which achieves this in part is described in the next section.

3.4 A New Fragmentation-Heat Transfer Model

In this section we develop a new model for heat transfer, allowing for a finite fragmentation rate, using the approach described in the previous section. Suppose that the melt surface area increases linearly for a time τ_f and then remains constant. This would be the case if a constant speed shock wave were instantaneously fragmenting a homogeneous region of mixture. In this case the $\dot{A}(t)$ function is given by

$$\dot{A}(t) = \frac{A_\infty}{\tau_f} \qquad 0 \leqslant t \leqslant \tau_f$$

$$= 0 \qquad t > \tau_f \tag{3.11}$$

Assuming a simple exponential decay law for the heat flux per unit area gives

$$Q = Q_0 \exp(-t/\tau_h) \tag{3.12}$$

Evaluating the integral in equation (3.10) using the models proposed in equations (3.11) and (3.12) gives

$$q(t) = Q_o A_\infty \frac{\tau_h}{\tau_f}\left[1 - \exp(-t/\tau_h)\right] \qquad 0 \leqslant t < \tau_f$$

$$= Q_o A_\infty \frac{\tau_h}{\tau_f}\left[\exp(-(t-\tau_f)/\tau_h) - \exp(-t/\tau_h)\right] \qquad t > \tau_f \tag{3.13}$$

The equation for q(t) is split into two parts because the solution changes when no <u>new</u> surface area is being formed. In the special case when $\tau_f = 0$ we have

$$q(t) = Q_o A_\infty \exp(-t/\tau_h) \tag{3.14}$$

The choice of values for Q_o and A_∞ is not arbitrary since there is a finite amount of energy in the melt which may be transferred to the sodium. Thus we must have

$$\int_o^\infty q(t)dt = m_m c_m (T_{mo} - T_{so}) = E_\infty \tag{3.15}$$

Writing equations (3.13) and (3.14) in terms of E_∞ gives

$\tau_f \neq 0$

$$q(t) = \frac{E_\infty}{\tau_f}\left[1-\exp(-t/\tau_h)\right] \qquad 0 \leqslant t \leqslant \tau_f$$

$$= \frac{E_\infty}{\tau_f}\left[\exp(-(t-\tau_f)/\tau_h) - \exp(-t/\tau_h)\right] \qquad t > \tau_f \tag{3.16}$$

$\tau_f = 0$

$$q(t) = \frac{E_\infty}{\tau_h}\exp(-t/\tau_h)$$

The heat flux per unit of available energy ($q(t)/E_\infty$) is plotted against time as a function of τ_f and τ_h in figures 3.4 - 3.7. Figure 3.4 shows the case of instantaneous fragmentation, for which the heat flux falls monotonically with time, with the rapidity of the fall determined by the value of τ_h. When $\tau_f \neq 0$ the heat flux increases with time for $t < \tau_f$, reaches a peak at $\tau = \tau_f$, when all the melt is fragmented, and then decays with time in a manner similar to the instantaneous fragmentation rate case.

The model described above has not been incorporated in CURLIM because it does not seem sensible to model the fragmentation/heat transfer processes to this degree of sophistication in the present simple model. To model fragmentation correctly it is necessary to allow for spatial variation of quantities, such as pressure. Also the present simple form for Q does not take into account directly the effect of the reduction in heat transfer caused by the fall in the temperature difference between the melt and sodium as heat is transferred. However, it does serve to illustrate the effect on heat transfer of including a finite fragmentation rate. Such calculations can be used as a guide to choosing reasonable bounds to the parameters controlling heat transfer in CURLIM. In addition, it is intended to explore the effect of including the type of model described above in a more sophisticated hydrodynamics code.

In the present model all the fragmented melt is assumed to be in the form of spherical particles of the same size. A recent paper by Doshi [13] presents results obtained using a Cho-Wright type model [8] to examine the effect of including a particle size distribution. He examined three different cases:

(i) all particles of the same size (185μm);

(ii) a uniform particle size distribution;

(iii) a lognormal particle size distribution obtained from experimental data.

The results obtained in the three different cases were not significantly different. For example, the efficiencies varied from 9.5% to 12.6% for the worst case. In other cases the difference was much smaller. The method of including a distribution of sizes is straightforward [13,14] but computationally more expensive. In view of

the other uncertainties in the model it does not seem necessary to include this modification at present.

3.5 A Mechanistic Heat Transfer Model for the Two Phase Region

In this section we describe a mechanistic model for heat transfer in the two phase region. Heat transfer is assumed to be due to radiation and conduction across the vapour film. The vapour present in the interaction zone is assumed to be located at the surface of the melt particles and to form a smooth vapour film. In this case it is easily shown [15] that the radiation heat flux per unit area is given by

$$Q = \sigma F (T_m^4 - T_s^4) \tag{3.17}$$

where the radiation view factor F is given by

$$F = \left[1/\varepsilon_m + (1 + \frac{\gamma}{R})^{-2} (\frac{1}{\varepsilon_s} - 1)\right]^{-1} \tag{3.18}$$

In the present study a melt emissivity of 0.84 is used [5]. A recent experimental study of the emissivity of liquid sodium for the temperature range 175°C to 520°C gave values of the emissivity of 0.045 - 0.057 [16]. In the absence of data at higher temperatures we assume a value of 0.06 in the present study.

The vapour film thickness is given by [13]:

$$\gamma = R\left(\left[\frac{1 + x m_s \rho_m}{m_m \rho_v}\right]^{1/3} - 1\right) \tag{3.19}$$

and the film boiling heat flux is then given by

$$Q = \frac{k_v}{\gamma} (T_m - T_s) \tag{3.20}$$

where k_v is the thermal conductivity of saturated vapour. A constant

value of 7×10^{-2} W/m K is used for the vapour thermal conductivity [17]. The total heat flux is obtained by adding the contributions from radiation and conduction across the vapour film.

The models described above were incorporated in CURLIM2 which use the diffusivity limited heat transfer model when melt is in contact with high-density sodium. Calculations using the new model for heat transfer in the two phase region were performed for the two cases given in Table 3.1. For the case of 250μm particles the new model gave an efficiency of 6.02% compared with 5.66% obtained by using a constant heat transfer coefficient ($10^3 W/m^2K$). For the case of 100μm particles the efficiency was increased from 8.42% to 9.27%. The calculations showed that the film boiling heat transfer coefficient was typically 4000 W/m^2K at the start of the calculation and fell to 100 W/m^2K at the end. The radiation heat transfer coefficient started at a value of 200 W/m^2K and increased to 1000 W/m^2K. The radiation heat transfer coefficient increases, even though the melt temperature is falling, because the temperature difference between the melt and sodium increases with time during the two phase stage of the calculation, as does the view factor term (equation (3.19)). Thus we may conclude that making the assumption that the heat transfer coefficient was equal to $10^3 W/m^2K$ during the two phase calculation was not very different from using a mechanistic model.

4. Heat Loss from the Interaction Zone

In this section we explore the effect of modelling heat loss from the interaction zone to the surrounding sodium and walls. This heat loss occurs because of condensation of sodium vapour and conduction of heat into the surrounding sodium or walls. The detailed modelling of these phenomena is beyond the scope of the present simplified model, but it is possible to allow for the heat loss by making simplifications.

Heat loss may be modelled by specifying a heat transfer coefficient from the sodium in the MFCI region to its surroundings. This heat loss term is split into two parts: heat loss to the slug; and heat loss to the side walls. Heat loss to the sodium slug is modelled using

$$q = -Sh_{top} (T_s - T_{so}) \qquad (4.1)$$

where S is the interfacial area between the slug and the interaction zone. Heat loss to the sidewalls above the initial MFCI zone is modelled using

$$q = - \frac{4m_s(\nu_s - \nu_{so})}{D_H} h_{side} (T_s - T_{so}) \qquad (4.2)$$

where D_H is the channel hydraulic diameter. In both the above equations the sink temperature was set equal to the initial sodium temperature, T_{so}, and it was assumed to remain fixed. The reduction in heat transfer which occurs as the surroundings heat up and temperature gradients form is ignored. Thus the present modelling will over-estimate the heat loss, for any given heat transfer coefficient.

4.1 Application to CURLIM

It proved to be a straight-forward task to include the heat loss terms in the sodium energy equation. The loss of sodium mass from the interaction zone due to vapour condensation was ignored. Table 4.1 below shows the effect of including heat loss for the base case calculation described in Appendix 1 of Reference 1.

h_{side} (W/m^2K)	h_{top} (W/m^2K)	efficiency (%)
0	0	8.86
10^3	10^3	8.81
10^4	10^4	8.44
10^5	10^5	6.19
0	10^5	8.61
10^5	0	6.34

Table 4.1: The Effect of Heat Loss on Efficiency

The data show that the inclusion of heat loss to the surroundings only has a significant effect if the heat transfer coefficient is assumed to take the rather high value of 10^5 W/m^2K. The data also show that in this geometry heat loss to the walls is much more important than heat loss

to the slug. This effect is geometry dependent, depending on the ratio of the slug surface area to the channel area exposed by expansion of the heated sodium.

It is not clear from the available literature what value the heat transfer coefficients in the loss terms should take. When vapour is present there will be condensation heat (and mass) transfer. However, both the theoretical and experimental data on this subject is limited. This is because of the experimental difficulty of measuring transient heat transfer rates, together with the amount of incondensible gas present (which has a considerable effect on the vapour mass transfer rate), and the uncertainty in the quoted values for the accommodation coefficient [12]. Fishlock [2] references data which suggests that a heat transfer coefficient of 4×10^4 W/m^{2}K may occur for sodium vapour condensing on cold clad, but it is not clear whether this is a peak value or some average value. Similarly it is not clear what value convective heat transfer coefficients should take. Clearly neither the flow nor the heat transfer process is fully developed, so that standard engineering correlations do not apply. Also the interfacial area between the slug and the interaction zone will be increased above the planar value by hydrodynamic instabilities. Thus in the absence of better data it is only possible to examine the effect of choosing a range of values in order to determine the importance of the effect.

Doshi [13] modelled heat loss to the surroundings by assuming the sodium and the cold walls could be modelled as two semi-infinite regions at uniform temperatures suddenly brought into contact with each other. He found that inclusion of this heat loss term had only a small effect on the calculated results, which is in agreement with the results obtained in the present study.

5. Hicks-Menzies Calculations

In this section we describe the use of CURLIM to perform improved Hicks-Menzies calculations. Hicks and Menzies [9] produced an effective upper bound on the efficiency with which thermal energy can be converted into mechanical energy. They considered the following two stage process:

(i) melt and coolant mix at constant volume to a common temperature and pressure;

(ii) this mixture expands at constant entropy to ambient pressure.

The work done is then simply the change in internal energy of the system during stage (ii). This calculation provides only an effective upper bound, since the first stage is not carried out isentropically, and thus, in theory, more work could be done. Hicks and Menzies made a number of simplifying assumptions in their calculations:

(i) they extrapolated the vapour-pressure curve into the supercritical region;
(ii) the vapour was treated as a perfect gas and the liquid was assumed to be incompressible;
(iii) A constant latent heat was used.

Various workers have attempted to improve upon the original work [10,11], mainly by using improved equations of state for sodium. However, to the author's knowledge the EOS based on the use of the thermal pressure coefficient has never been used for such calculations.

An option has been included in the CURLIM code to allow such calculations to be made. By setting IHM≠0 in the input data the code calculates the conditions achieved at the end of a constant volume mixing stage. The calculation is then continued using an inertial loading model. By setting the frictional and gravitational terms to zero, using a small time-step ($\sim 10^{-3}$ms), a massive slug (400m long) and a high heat transfer rate between the melt and sodium the expansion is approximately isentropic. The cover gas volume is made very large, so that the work done is equal to the kinetic energy of the slug when the mixture has expanded down to the chosen end-state pressure (usually 0.1MPa). In addition this model can be used to examine the maximum effect of the metal-insulator transition or vapour blanketing, by terminating heat transfer appropriately.

Table 5.1 below shows the conditions at the end of the constant volume mixing phase, the Hicks-Menzies type efficiency, and the efficiency and final melt temperature when a metal-insulator transition is applied at

a specific volume of $2 \times 10^{-3} m^3/kg$ together with vapour blanketing, as a function of melt/sodium mass ratio. The efficiency is defined as the work done by the melt divided by the melt thermal energy above the sodium saturation temperature.

m_m/m_s (-)	T_{init} (K)	P_{init} (MPa)	η (%)	T_{cut} (K)	η_{mod} (%)
0.5	1627	354	25.8	1609	22.9
1	1940	589	35.4	1882	28.4
2	2332	882	41.0	2192	28.1
3	2566	1058	40.7	2379	23.8
5	2833	1259	38.0	2584	16.4
7.5	3009	1391	31.2	2722	11.6
10	3111	1467	25.6	2801	8.8
15	3226	1553	17.3	2888	5.8
20	3288	1600	10.5	2936	4.3

Table 5.1: Results from the Hicks-Menzies type calculations

The data in the above table show that the pressure at the end of the constant volume mixing stage is unrealistically high and that supercritical temperatures occur for melt/sodium mass ratios above about 2. The efficiency data is displayed in figure 5.1. The peak efficiency is approximately 41% and occurs for a melt/sodium mass ratios of ~ 2-3. The calculation which assumed heat transfer to be terminated by vapour blanketing or a metal-insulator transition gives a peak efficiency of 29%, which occurs for melt/sodium mass ratios ~ 1-2. In this case the final melt temperature is of the order of 2000K, which is still 900K above the sodium saturation temperature. For higher melt/sodium mass ratios the final melt temperature is even higher, so that a considerable amount of thermal energy is available to produce more vapour.

Figure 5.2 compares the results from the present work with those obtained in the original study by Hicks and Menzies. Note that in this figure the efficiency is plotted against the sodium/melt mass ratio, as

used in the original paper. The figure shows that the peak efficiency is very similar in both cases but that this peak occurs for mixtures consisting of 3-4 times more sodium than predicted by Hicks and Menzies [9]. Thus it may be concluded that improving the EOS has only changed the composition of the optimum mixture and not reduced the efficiency.

The present calculations have highlighted the non-physical nature of the first stage of the process which produces pressure of the order of 1000 MPa, compared to pressures of the order of 20-100 MPa in more realistic simulations which allow for finite energy transfer rates and acoustic pressure relief. It is not clear that it is sensible to use effects such as the metal-insulator transition in calculations which use such unphysical thermodynamic trajectories.

6. Conclusions

In this paper we have presented some modifications to CURLIM, a rate limited MFCI model for sodium. The modifications include an improved heat transfer model, a model of heat loss from the interaction zone, and modification of the modelling of the acoustic loading phase.

A model has been constructed which accounts for the transmission of rarefaction waves into the interaction zone. Calculations show that the choice of behaviour upon return of rarefaction waves from the free surface (either transmission or reflection) does not change the predicted efficiencies significantly.

A diffusivity limited heat transfer model proposed by Cho et al [8] has been implemented and used to make upper bound calculations for the situation of instantaneous fragmentation of the melt. These calculations have shown that in some cases the efficiency is considerably reduced compared to assuming a heat transfer coefficient between the melt and sodium of 10^7 W/m^{2}K and in other cases the efficiency is comparable. In all cases the peak pressure was reduced and vapour was formed at a lower sodium specific volume, altering the effect of the possible metal-insulator transition in sodium. A model capable of allowing for the effect of a finite fragmentation rate has been developed and explored. A mechanistic model of heat transfer in the two phase region has been formulated and implemented.

The effect of heat loss from the interaction zone has been examined. Models of heat loss to the sodium slug and cold walls have been included. Calculations suggest that allowing for heat loss only reduces the efficiency significantly (for the geometry of the chosen example) if the rather high heat transfer rate of 10^5 W/m^2K is used.

CURLIM has been used to perform improved Hicks-Menzies type thermodynamic limit calculations. A peak efficiency of 41% (based on excess thermal energy above the sodium saturation temperature) was obtained. This value is comparable with the value obtained in the original study by Hicks and Menzies but occurs for a sodium/melt mass ratio differing by a factor of about 3. Calculations including vapour-blanketing and the metal-insulator transition have also been carried out and were found to give a peak efficiency of 28%.

In a future paper it is intended to present the results of an uncertainty study to be carried out in order to determine which areas of the modelling have most effect on the MFCI characteristics predicted by CURLIM.

Acknowledgements

The author would like to thank Mr I Cook and Dr A Thyagaraja (Culham) and Dr J B Knowles (Winfrith) for useful discussions during the course of this work. The author would also like to thank Mrs.E.Barnham for her accurate typing of this manuscript.

References

[1] Fletcher, D.F., CURLIM: A rate limited MFCI model for sodium, Part I: Fundamental model and parameter studies. CLM-R262 (1986).

[2] Fishlock, T.P., EXPEL - A computing module for molten fuel/coolant interactions in fast reactor sub-assemblies. AEEW-R1029 (1975).

[3] Roberts, J.K., Heat and Thermodynamics, Blackie and Sons, London (1928).

[4] Browning, P., An equation of state for sodium. AERE-R9847 (1981).

[5] Fink, J.K., Chasanov, M.G., and Leibowitz, L., Thermodynamic properties of uranium dioxide, ANL-CEN-RSD-80-3 (1981).

[6] Fletcher, D.F., Modelling the Transient pressurization during a molten fuel coolant interaction. AEEW-M2126 (1984).

[7] Curle, N. and Davies, H.J., Modern fluid dynamics, Vol 2, Compressible flow, Van Norstrand Reinhold, London. (1971).

[8] Cho, D.H., Ivins, R.O. and Wright, R.W., A rate-limited model of molten fuel/coolant interactions: Model development and preliminary calculations, ANL-7919 (1972).

[9] Hicks, E.P. and Menzies, D.C., Theoretical studies of the fast reactor maximum accident. ANL-7120 (1965).

[10] Judd, A., Calculations of the thermodynamic efficiency of molten fuel coolant interactions. Trans. ANS, Vol.13. p.369-370 (1970).

[11] Padilla, A., Analysis of mechanical work energy for LMFBR maximum accidents. Nucl. Tech., vol.12, p.348-355. (1971).

[12] Rohsenow, W.M., Film condensation of liquid metals. In Progress in Heat and Mass Transfer, Vol.7, edited by O.E.Dwyer, Pergamon Press, Oxford, (1973).

[13] Doshi, J.B., An improved model for the molten fuel coolant interaction incorporating the particle size distribution, fission heating and heat loss to cold structure. Paper presented at the conference on the science and technology of Fast Reactor Safety, Guernsey, U.K., May 12-16, 1986.

[14] Fletcher, D.F., Modelling transient energy release from molten fuel coolant interaction debris. AEEW-M2125 (1984).

[15] Sparrow, E.M. and Cess, R.D., Radiation heat transfer. Hemisphere Publishing Corporation, Washington. (1978).

[16] Hattori, N et al., Emissivity of liquid sodium. Heat Transfer Jap. Res. Vol.13, p 30-40 (1984).

[17] Caldorola, L., A theoretical model for the molten fuel sodium interaction in a nuclear fast reactor. Nucl. Eng. and Design, Vol.22, p.175-211 (1972).

Appendix 1: A Derivation of the Reflection Model.

In this Appendix we give a derivation of equation 3.4 of reference 1 in order to show that this is applicable to the situation where a reflection boundary condition is applied. Consider a (sodium) slug of length L, initially at rest, with pressure boundary conditions of

$$p(0,t) = h(t)$$
$$p(L,t) = 0 \qquad \text{(A1.1)}$$

It is easily shown [7] that an acoustic wave satisfies the following equations

$$\frac{\partial^2 p}{\partial z^2} = \frac{1}{c^2}\frac{\partial^2 p}{\partial t^2} \qquad \text{(A1.2)}$$

$$\frac{\partial v}{\partial t} = -\frac{1}{\rho}\frac{\partial p}{\partial z} \qquad \text{(A1.3)}$$

where:
- p = pressure
- v = particle velocity
- c = sound speed
- ρ = density
- z = space-coordinate
- t = time

Taking Laplace transforms of equations (A1.2) and (A1.3) gives

$$\frac{\partial^2 \bar{p}}{\partial z^2} = \left(\frac{s}{c}\right)^2 \bar{p} \qquad \text{(A1.4)}$$

and $$s\bar{v} = -\frac{1}{\rho}\frac{\partial \bar{p}}{\partial z} \qquad \text{(A1.5)}$$

where $\bar{g}$ denotes the transform of g. Applying the boundary conditions and setting z = 0 gives

$$\bar{v} = \frac{\bar{h}}{\rho c} \coth(s\tau) \qquad \text{(A1.6)}$$

where $\tau = L/c$.

Expanding $\coth(s\tau) = 1 + 2\sum_{n=1}^{\infty} e^{-2ns\tau}$

and inverting the transform gives

$$v(t) = \frac{h(t)}{\rho c} + \frac{2}{\rho c} \sum_{n=1}^{\infty} \int_0^t h(\bar{t})\,\delta(t-\bar{t}-2n\tau)\,d\bar{t} \qquad \text{(A1.7)}$$

Comparison of equation (A1.7) with equation (3.4) of reference 1 shows that they give the same expression for v as a function of p (allowing for an additive constant). The above expression (equation (A1.7)) was derived by assuming that p(t) is known at z=0 and is not changed by the acoustic waves incident upon the boundary. This is a reflection boundary condition; p is not changed by the rarefaction wave, only the particle velocity is changed.

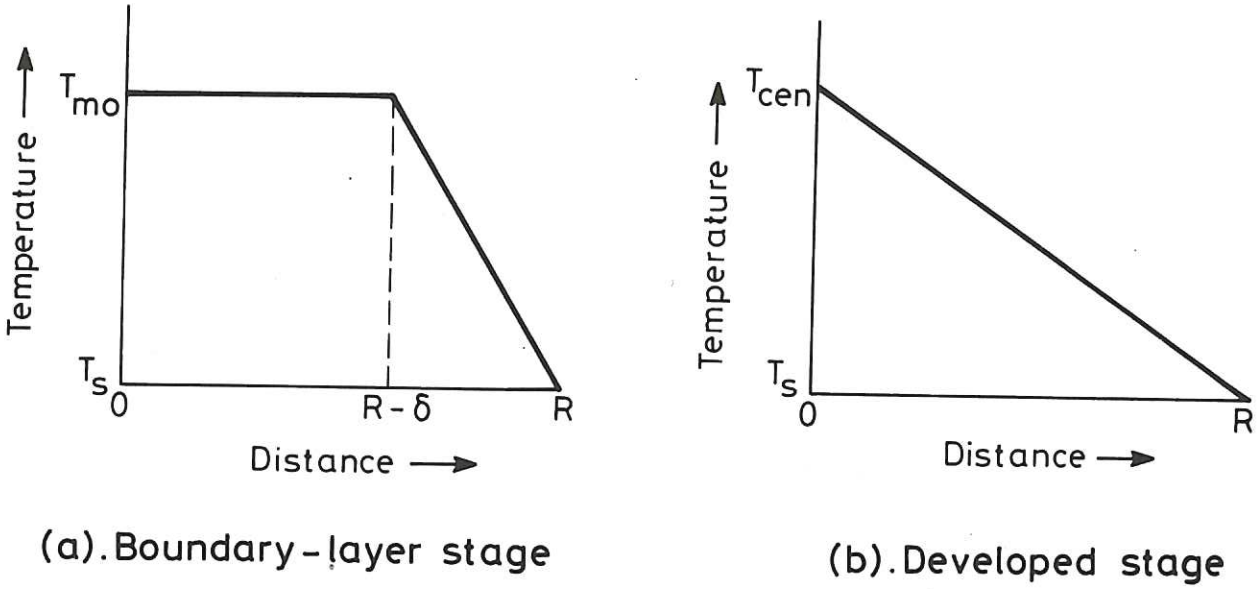

Fig. 3.1 The temperature profile used in the diffusivity limited heat transfer model.

CLM-R267

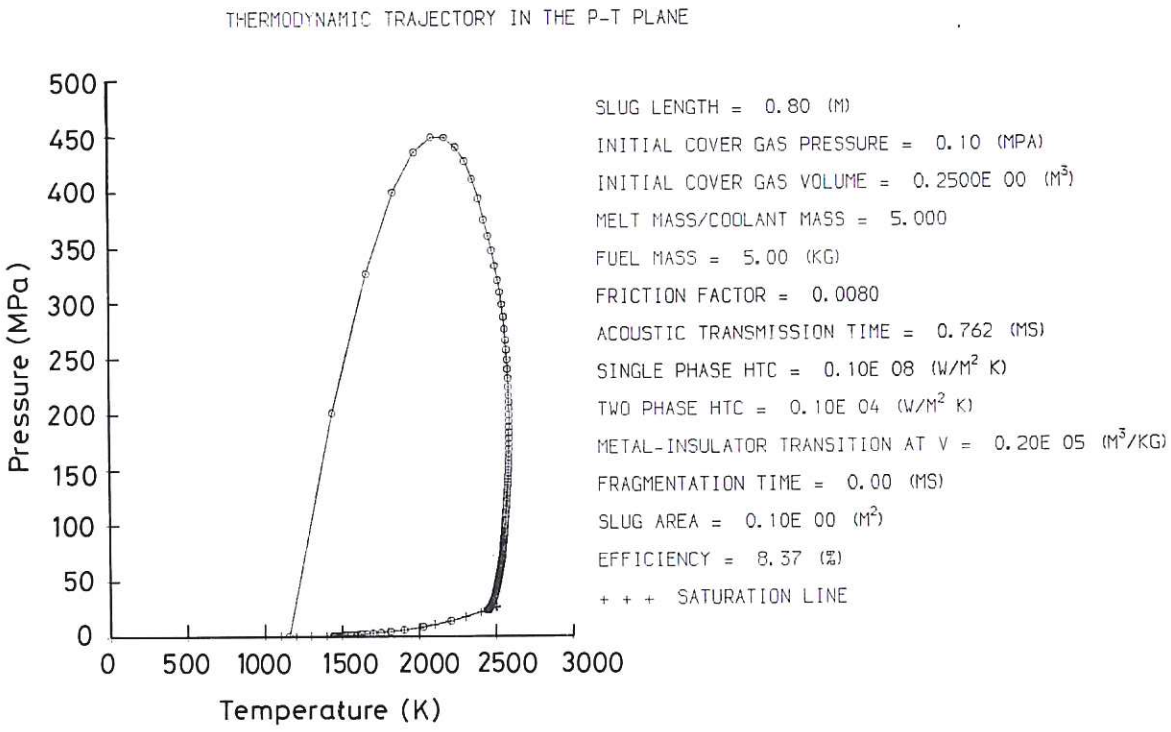

Fig. 3.2 A typical calculation using the old heat transfer model.

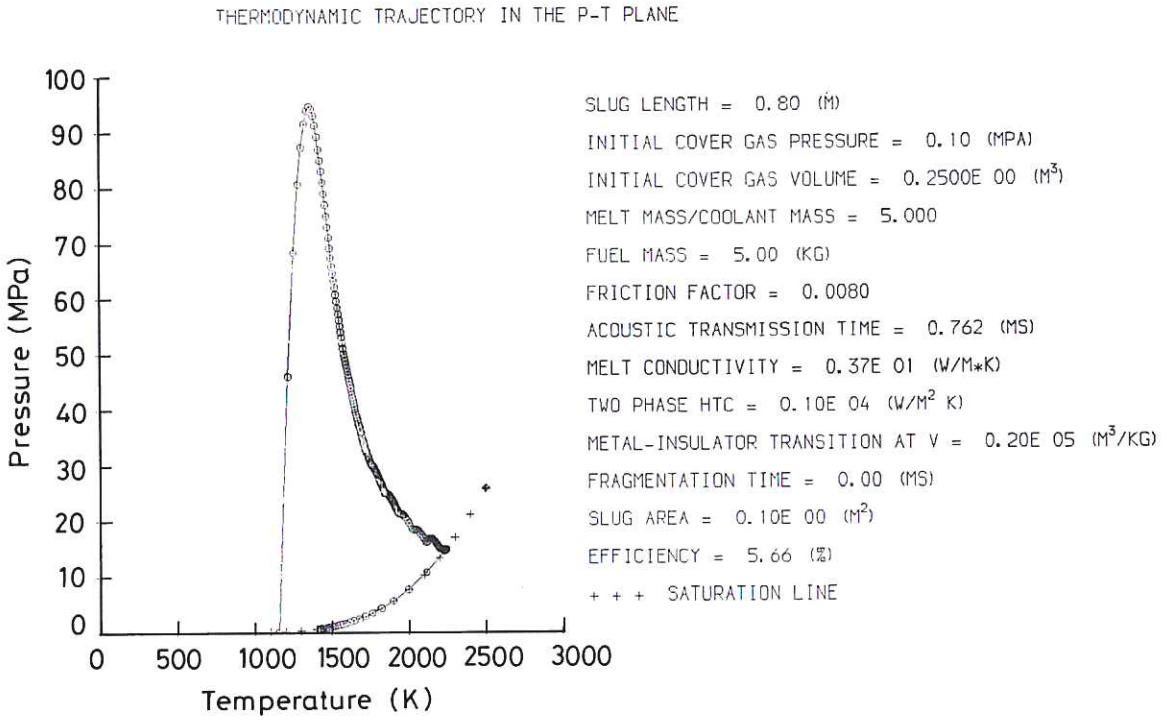

Fig. 3.3 A typical calculation using the new transfer model.

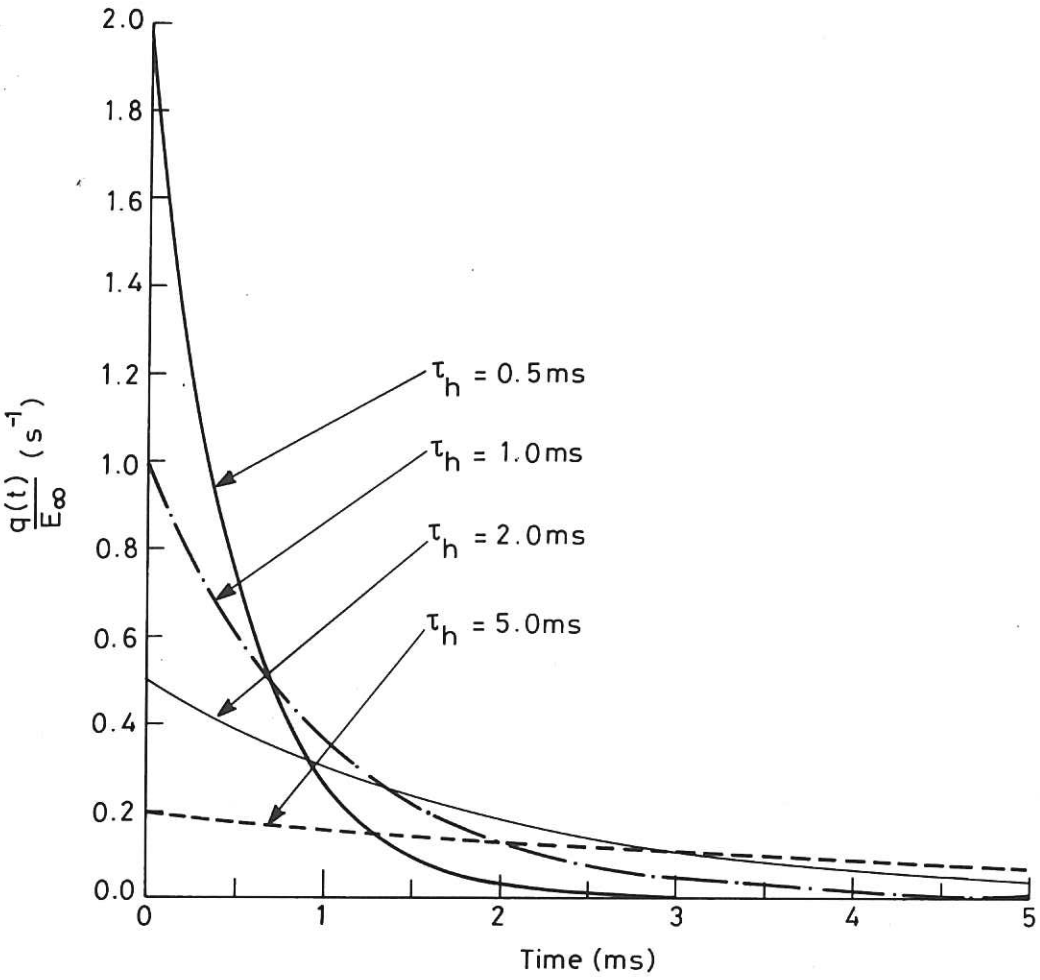

Fig. 3.4 The heat transfer rate against time for τ_f=0.

CLM-R267

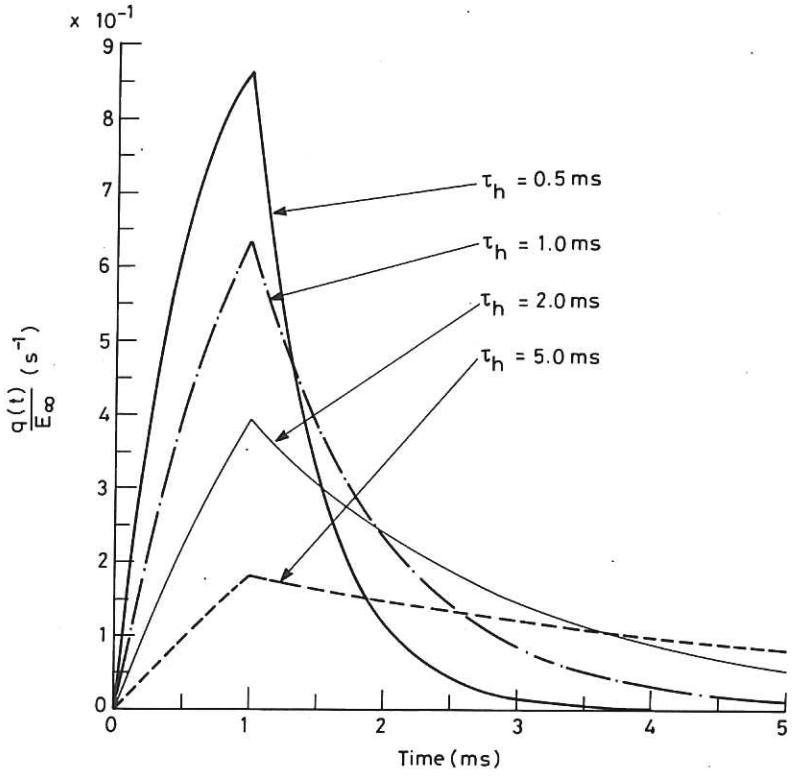

Fig. 3.5 The heat transfer rate against time for τ_f=1.0ms.

CLM-R267

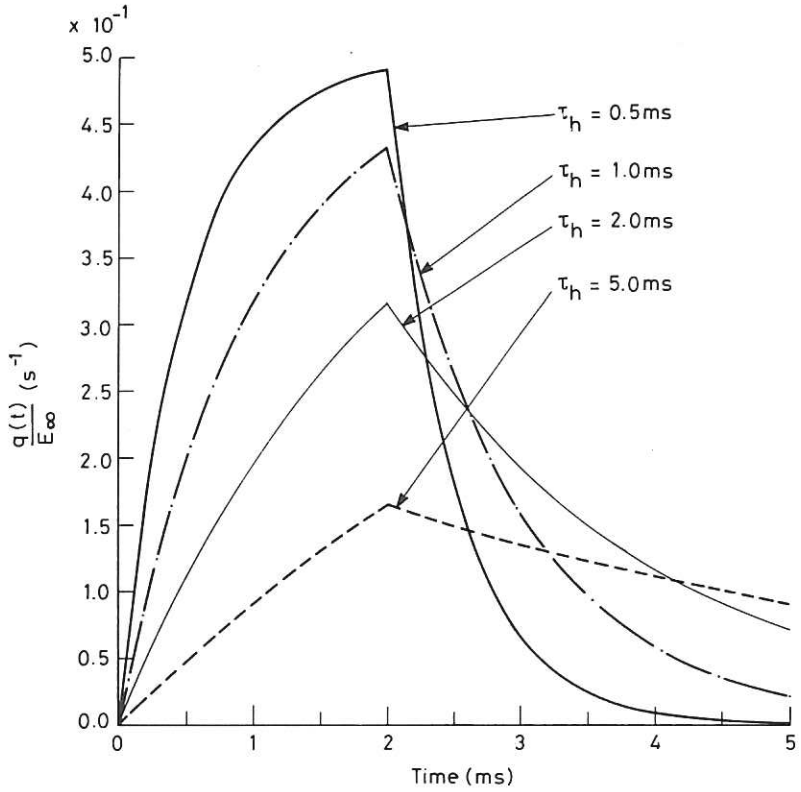

Fig. 3.6 The heat transfer rate against time for τ_f=2.0ms.

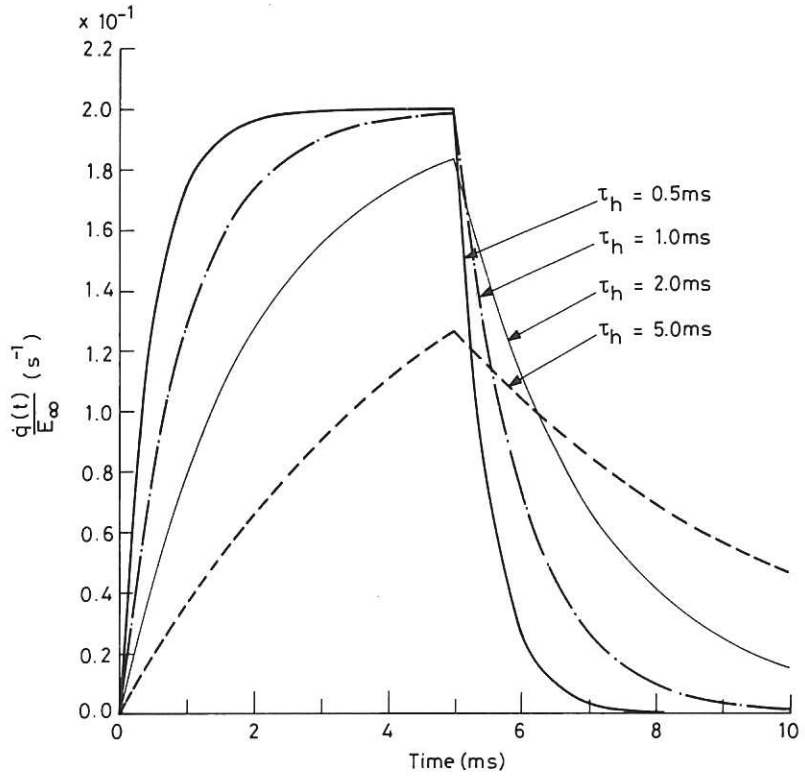

Fig. 3.7 The heat transfer rate against time for τ_f=5.0ms.

CLM-R267

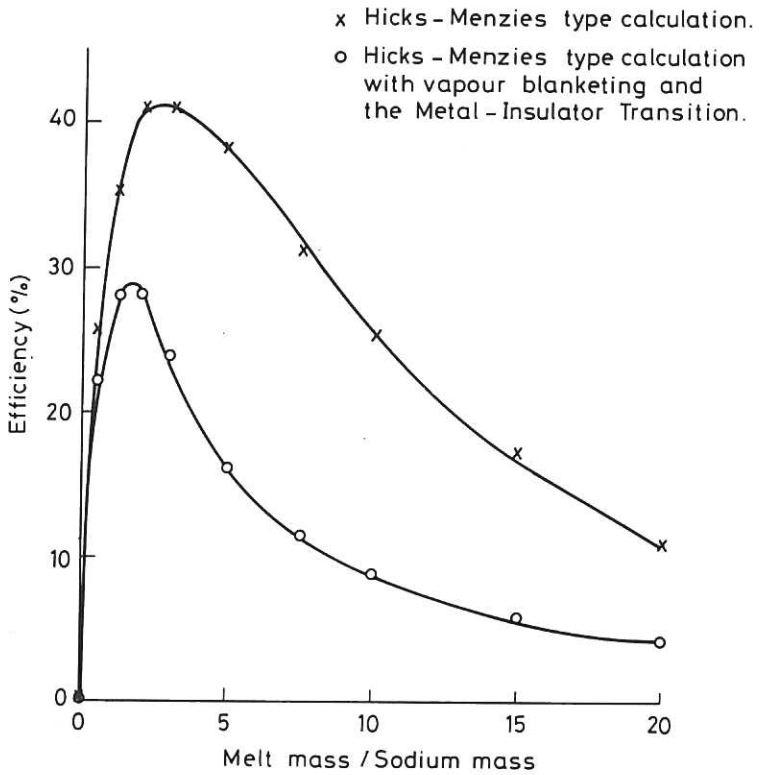

Fig. 5.1 Hicks-Menzies calculation using the EOS used in curlim.

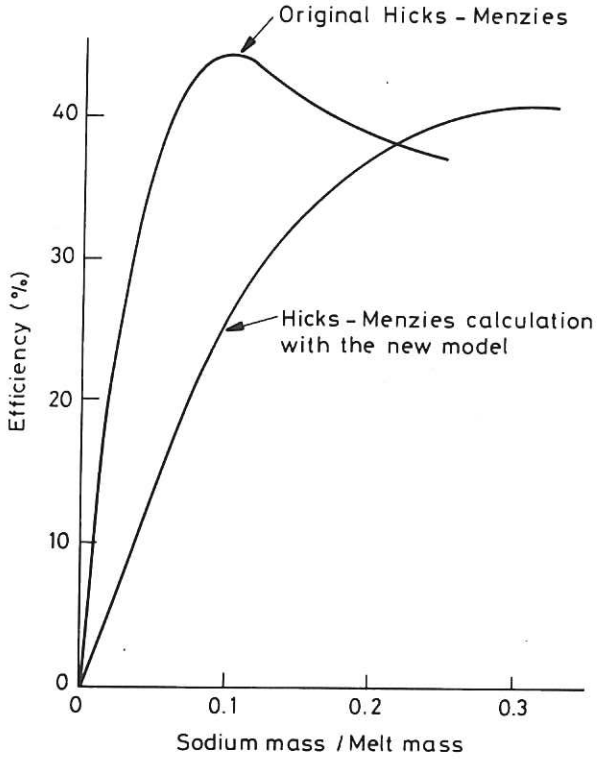

Fig. 5.2 Comparison of the present results with those of Hicks and Menzies.

Available from
HER MAJESTY'S STATIONERY OFFICE
49 High Holborn, London, WC1V 6HB
(Personal callers only)
P. O. Box 276, London, SE1 9NH
(Trade orders by post)
13a Castle Street, Edinburgh, EH2 3AR
41 The Hayes, Cardiff, CF1 1JW
Princess Street, Manchester, M60 8AS
Southey House, Wine Street, Bristol, BS1 2BQ
258 Broad Street, Birmingham, B1 2HE
80 Chichester Street, Belfast, BT1 4JY

PRINTED IN ENGLAND